Nonlinear Transient Analysis of Shells and Solids of Revolution by Convected Elements

TED BELYTSCHKO* AND B. J. HSIEH†
University of Illinois at Chicago Circle, Chicago, Ill.

A convected coordinate scheme is employed for the development of a finite element procedure for large-displacement, small strain, elastic-plastic, dynamic problems. In this scheme, the element's convected coordinates rotate, but do not deform, with the elements. The strains can be linearly related to the displacement of the element relative to the convected coordinates, and similarly, the nodal forces can be simply related to the element stresses. Hence the scheme is computationally quite efficient, particularly for elements such as shells, where numerical quadrature through the thickness is required. The method is applied here to conical shell and axisymmetric triangular continuum elements, and results are presented for several problems.

Nomenclature

$\{\ \}$ = column matrix
$[\ ]$ = rectangular matrix
$[\ ]^T$ = matrix transpose
$\{d\}, \{d\}_I$ = global and local nodal displacements, respectively
$\{\ddot{d}\}$ = nodal accelerations
E, E_p = elastic and plastic modulus, respectively
$[E^p], \{E^c\}^T$ = strain-nodal displacement matrix for r–z plane and circumferential strains, respectively
$\{f^p\}, \{f^c\}$ = nodal forces due to planar and circumferential stresses, respectively
$\{F^{\text{ext}}\}$ = nodal forces due to applied loads
$[L]_I$ = connectivity matrix for element I
m_i^p, m_i^c = moment at node i due to planar and circumferential stresses, respectively
$[M]$ = mass matrix
r_i, z_i = nodal coordinates of an element relative to node 1
r, z, θ = fixed coordinates
$\hat{r}, \hat{z}, \theta$ = convected coordinates
$[T]$ = transformation matrix for nodal displacements
$\{u\}$ = $\{u_r, u_z\}^T$, displacement field
V, V_I = total volume and volume of element I, respectively
$\hat{x}, \hat{y}$ = convected coordinates for shell element
α = angle of rigid body rotation in element
β = angle of inclination of conical shell element
Δt = time step
$\delta(\ )$ = variation
$\{\hat{\varepsilon}\}$ = $\{\hat{\varepsilon}_r, \hat{\varepsilon}_z, 2\hat{\varepsilon}_{rz}\}^T$, strains in r–z plane in convected coordinates
ε_θ = circumferential strain
$\hat{\varepsilon}_m$ = midplane axial strain in shell element
$[\lambda]$ = transformation matrix for displacement field
$\{\hat{\sigma}\}$ = $\{\hat{\sigma}_r, \hat{\sigma}_z, \hat{\sigma}_{rz}\}^T$, stresses in r–z plane
σ_o, σ_u = yield stress and ultimate stress, respectively
σ_θ = circumferential stress
$\phi, \hat{\phi}$ = rotation of shell cross section relative to fixed and convected coordinates

I. Introduction

ONE of the major difficulties in the finite element analysis of the nonlinear transient response of structures and continua is their excessive computational requirements. As a consequence, economical considerations usually severely restrict the size of meshes, and the analysis of realistic engineering models is hampered considerably. In response to these difficulties, several investigators have recently studied techniques such as interpolation (Stricklin et al.[1]) and the applicability of explicit integration schemes (Krieg and Key[2]).

A complete review of nonlinear transient finite element techniques is beyond the scope of this paper; such reviews may be found in Oden[3] and Stricklin et al.[4] Work published since these reviews are McNamara and Marcal,[5] Wu and Witmer,[6] and Hartzman and Hutchinson.[7] The latter is noteworthy in that it employs a semi-Eulerian description which, compared to the more common Lagrangian descriptions, simplifies the finite element relations. However, Eulerian formulations present difficulties in anisotropic or inhomogeneous materials and when applied to structural elements such as beams.

This paper, and a previous work of the authors,[8] explore another source of computational improvement: the use of convected coordinate procedures. In these schemes, each element is associated with a coordinate system that rotates but does not deform with the element. For problems with small strains but large rotations, which probably encompasses a large portion of nonlinear engineering problems, it can be shown that the strains are linearly related to what are termed "deformation displacements." The latter are simply the displacements of the element relative to the convected coordinates. Similarly, within the convected coordinates the nodal forces are simply related to the stresses. The important nonlinearities which arise from large rotations are accounted for entirely by transformations between the global and convected coordinates and the omission of the rigid body motion in the strain-displacement relations. Hence, the computation of nodal forces is considerably simplified, particularly in elements where numerical quadrature is required.

Convected coordinate procedures have been used in static finite element analysis by several investigators, among them, Argyris et al.,[9] Wempner,[10] and Murray and Wilson.[11] The formulation given herein differs somewhat from the work of Argyris et al. in that formulas are developed for total nodal forces rather than linearized increments. This may be of advantage in dynamic problems for it eliminates one source of truncation error.

Convected coordinate procedures, to the best of the authors' knowledge, were first applied in nonlinear, transient finite element methods in Ref. 8. In that paper, the method was applied to two-dimensional beams and continuum elements and the formulation was restricted to elements which are simply connected from a topological viewpoint. In this paper, the formulation is extended to the multiply connected elements such as found in axisymmetric analysis. Detailed formulations are given for the toroidal, continuum element and the conical shell element in Sec. III, and sample results are presented in Sec. IV.

Presented as Paper 73-359 at the AIAA/ASME/SAE 14th Structures, Structural Dynamics, and Materials Conference, Williamsburg, Va., March 20–22, 1973; submitted April 6, 1973; revision received February 20, 1974. The support of the National Science Foundation under Grant GK 5834 and the computer time provided by the University of Illinois at the Chicago Circle Computer Center is gratefully acknowledged.

Index category: Structural Dynamic Analysis.

* Associate Professor of Structural Mechanics, Department of Materials Engineering.

† Research Assistant.

II. Finite Element Equations

The finite element equations are obtained by the principle of virtual work with inertial forces included in a d'Alembert sense:

$$\int(\{\delta\hat{\varepsilon}\}^T\{\hat{\sigma}\} + \delta\varepsilon_\theta\sigma_\theta)dV = \{\delta d\}^T(\{F^{\text{ext}}\} - [M]\{\ddot{d}\}) \quad (1)$$

Here the right- and left-hand sides represent the variations of external and internal work. The internal work is separated into that due to strains in the r–z plane and that due to circumferential strains. Stresses and strains in the r–z plane, $\{\hat{\sigma}\}$ and $\{\hat{\varepsilon}\}$, respectively, are measured in the convected coordinates which rotate with the element in the r–z plane. Because of the toroidal nature of axisymmetric elements, rotations and translations in the r–z plane are not strictly rigid body motions. However, in the computation of the first part of the internal work, such motions can be treated as rigid body motions because they produce only circumferential strains ε_θ without any strains in the r–z plane. Therefore, the term "rigid body motion" is used in this paper to refer to such motions.

To find this rigid body motion of the element $\{u^{\text{rig}}\}$, the angle of rotation must be known. Formulas for the rigid body rotation can be obtained by means of the polar decomposition theorem. In simplex elements,[3] the rigid body rotation is constant. For nonsimplex elements these formulas will be approximate since the rigid body rotation is not constant in higher order elements. Once the rigid body component of the motion is known, the deformation displacements are obtained by

$$\{u^{\text{def}}\} = \{u\} - \{u^{\text{rig}}\} \quad (2)$$

This additive decomposition of displacements is of course not possible for a continuum. Only when the continuum is subdivided into elements with constant or slightly varying rotations is this decomposition feasible. The convected strains are then given in terms of the deformation displacements by

$$\begin{Bmatrix} \hat{\varepsilon}_r \\ \hat{\varepsilon}_z \\ 2\hat{\varepsilon}_{rz} \end{Bmatrix} = \begin{bmatrix} \partial/\partial\hat{r} & 0 \\ 0 & \partial/\partial\hat{z} \\ \partial/\partial\hat{z} & \partial/\partial\hat{r} \end{bmatrix} \begin{Bmatrix} \hat{u}_r^{\text{def}} \\ \hat{u}_z^{\text{def}} \end{Bmatrix} \quad (3)$$

where displacements in the convected and global coordinates are related by the usual orthogonal transformation

$$\{\hat{u}\} = [\lambda]\{u\}, \quad \{d\} = [T]\{d\} \quad (4)$$

Since the rigid body motion has been eliminated in obtaining the deformation displacements, as long as the strains and the variation of rotations within an element are small, the preceding formulas are applicable regardless of the magnitude of the rotations.

The circumferential strains are computed by the linear relation

$$\varepsilon_\theta = u_r/r \quad (5)$$

The use of the linear relation for the hoop strain is standard for nonlinear analysis,[4] but it limits the analysis to moderate radial displacements.

For a generic element I, the strain-displacement equations can be expressed in the matrix form

$$\begin{aligned} \{\hat{\varepsilon}\} &= [E^p]_I\{\hat{d}^{\text{def}}\}_I \\ \varepsilon_\theta &= \{E^c\}_I\{d\}_I \end{aligned} \quad (6)$$

where $\{d\}_I$ are the nodal displacements of the element.

If we insert Eq. (6) into Eq. (1), we find

$$\sum_I \{\delta\hat{d}^{\text{def}}\}_I^T\int_{V_I}[E^p]_I^T\{\hat{\sigma}\}dV + \{\delta d\}_I^T\int_{V_I}\{E^c\}_I\sigma_\theta dV = \{\delta d\}^T(\{F^{\text{ext}}\} - [M]\{\ddot{d}\}) \quad (7)$$

Taking the variation of Eq. (4), we find

$$\{\delta\hat{d}^{\text{def}}\}_I = [T]\{\delta d^{\text{def}}\}_I \quad (8)$$

If we define internal nodal forces due to planar and circumferential stresses by

$$\begin{aligned} \{f^p\}_I &= [T]^T\int_{V_I}[E^p]_I^T\{\hat{\sigma}\}dV \\ \{f^c\}_I &= \int_{V_I}\{E^c\}_I^T\sigma_\theta dV \end{aligned} \quad (9)$$

and make use of Eq. (8), then Eq. (7) can be written

$$\sum_I[\{\delta d^{\text{def}}\}_I^T\{f^p\}_I + \{\delta d\}_I^T\{f^c\}_I] = \{\delta d\}^T(\{F^{\text{ext}}\} - [M]\{\ddot{d}\}) \quad (10)$$

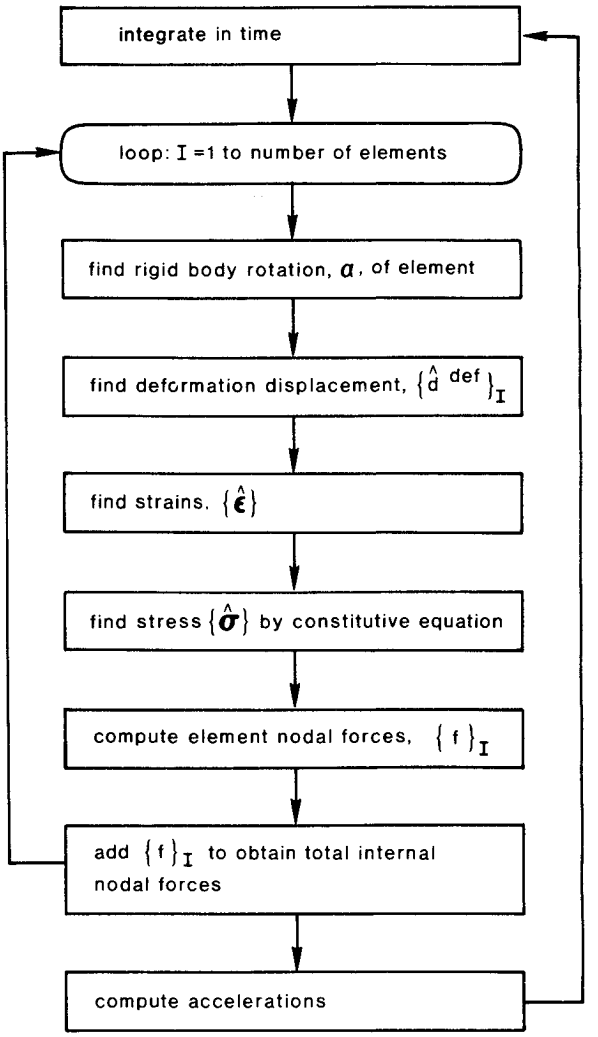

Fig. 1 Flow chart.

The nodal forces $\{f^p\}_I$ are self-equilibrated, hence

$$\{\delta d^{\text{rig}}\}_I^T\{f^p\}_I = 0 \quad (11)$$

Also, the element nodal displacements can be related to the total nodal displacement vector by the connectivity matrix[3]

$$\{d\}_I = [L]_I\{d\} \quad (12)$$

If we add Eqs. (11) to (10), use Eq. (12) and the arbitrariness of $\{\delta d\}$, we obtain the governing equations of the system

$$\{\ddot{d}\} = [M]^{-1}(\{F^{\text{ext}}\} - \sum_I[L]_I(\{f^p\}_I + \{f^c\}_I)) \quad (13)$$

A flow chart of the computational procedure is shown in Fig. 1. The program uses a central difference explicit integration procedure and a lumped mass matrix. The efficacy of this combination in impulsively loaded problems has been amply demonstrated by Krieg and Key.[2]

III. Elements

Two elements have been incorporated in the computer program: 1) a linear displacement, triangular, torodial continuum element and 2) a conical shell element. These elements are shown in Fig. 2, along with the nomenclature used in this paper.

The triangular element is the standard simplex element; its displacement field relative to node 1 is given by

$$\begin{Bmatrix} u_r \\ u_z \end{Bmatrix} = \begin{bmatrix} a_1 & a_2 \\ a_3 & a_4 \end{bmatrix} \begin{Bmatrix} \hat{r} \\ \hat{z} \end{Bmatrix} \quad (14)$$

The angle of rigid body rotation α is constant in the element and computed by the formula:

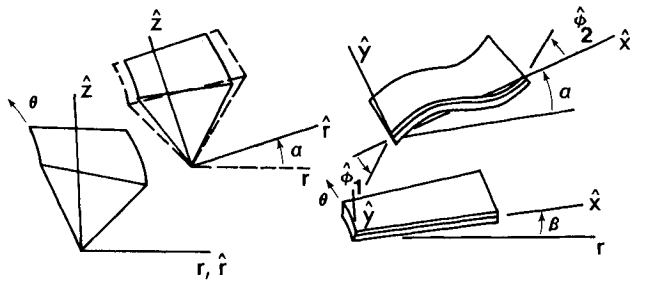

Fig. 2 Axisymmetric triangular continuum and conical shell elements.

$$\tan\alpha = \frac{a_3 - a_2}{2 + a_1 + a_4} = \frac{\hat{z}_3 D_{z2} - \hat{z}_2 D_{z3} + \hat{r}_3 D_{r2} - \hat{r}_2 D_{r3}}{4A + \hat{z}_3 D_{r2} - \hat{z}_2 D_{r3} - \hat{r}_3 D_{z2} + \hat{r}_2 D_{z3}} \tag{15}$$

where A is the area of the element, (r_i, z_i) the nodal coordinates relative to node 1, and (D_{ri}, D_{zi}) the nodal displacements relative to the displacement of node 1. The deformation nodal displacements are found at each node by subtracting the nodal displacements which correspond to the rigid body rotation α. They are

$$\begin{Bmatrix} \hat{D}_{ri} \\ \hat{D}_{zi} \end{Bmatrix}^{\text{def}} = [\lambda] \begin{Bmatrix} D_{ri} \\ D_{zi} \end{Bmatrix} - ([I] - [\lambda]) \begin{Bmatrix} r_i \\ z_i \end{Bmatrix} \tag{16}$$

where

$$[\lambda] = \begin{bmatrix} \cos\alpha & \sin\alpha \\ -\sin\alpha & \cos\alpha \end{bmatrix} \tag{17}$$

In Eq. (16), the first right-hand term corresponds to the total displacements in the convected coordinates, while the second term represents the displacements due to rigid body rotation. The translations have been omitted by defining $\{D\}$ as the displacement relative to node 1.

Using Eq. (3), it follows that the r–z strains in the convected coordinates are then related to the deformation nodal displacements by

$$\begin{Bmatrix} \hat{\varepsilon}_r \\ \hat{\varepsilon}_z \\ 2\hat{\varepsilon}_{rz} \end{Bmatrix} = \frac{1}{2A} \begin{bmatrix} \hat{z}_3 & 0 & -\hat{z}_2 & 0 \\ 0 & -r_3 & 0 & \hat{r}_2 \\ -\hat{r}_3 & \hat{z}_3 & \hat{r}_2 & -\hat{r}_2 \end{bmatrix} \begin{Bmatrix} \hat{D}_{r2} \\ \hat{D}_{z2} \\ \hat{D}_{r3} \\ \hat{D}_{z3} \end{Bmatrix}^{\text{def}} \tag{18}$$

The circumferential strain ε_θ is related to the total radial displacement by Eq. (5). Once all the strains are known, the stresses are computed by the stress-strain law, which, because both stresses and strains are measured in the convected coordinates, is independent of the rotation.

The $[E^p]$ matrix is defined by Eq. (18), while the standard relation between ε_θ and u_r defines the $[E^c]$ matrix. The nodal forces can then be found by a direct application of Eq. (9), which yields

$$\begin{Bmatrix} f^p_{2x} \\ f^p_{2y} \\ f^p_{3x} \\ f^p_{3y} \end{Bmatrix} = \begin{bmatrix} [\lambda]^T & [0] \\ [0] & [\lambda]^T \end{bmatrix} \int_{V_l} [E^p]_l^T \{\hat{\sigma}\} dV \tag{19a}$$

$$f^p_{1x} = -(f^p_{2x} + f^p_{3x}) \quad f^p_{1y} = -(f^p_{2y} + f^p_{3y}) \tag{19b}$$

$$\{f^c\} = \int_{V_l} [E^c]_l^T \sigma_\theta \, dV \tag{19c}$$

The integrands in Eqs. (19) are not constant, but a one point integration has been found to be adequate.

In the conical shell element the convected $\hat{x}$ axis is taken to lie along the line joining the nodes. Cubic polynomial shape functions in $\hat{x}$ are used for the transverse displacements, linear shape functions for the axial displacements. The rotation is not constant within this type of element, but if the rotation relative to the $\hat{x}$ axis is small, then the rotation of the $\hat{x}$ axis, α, should be a good approximation of the rotation component of the element's displacement.

The deformation displacements are then the nodal rotations relative to the $\hat{x}$ axis

$$\hat{\phi}_i = \phi_i - \alpha \tag{20}$$

and the midplane displacement, which can immediately be expressed in terms of the midplane strain $\hat{\varepsilon}_m$.

The strain-displacement equations are

$$\hat{\varepsilon}_x = \hat{\varepsilon}_m - \hat{y}\,\partial\hat{\phi}(\hat{x})/\partial\hat{x} \tag{21a}$$

$$\varepsilon_\theta = (1/r)[u_r - \hat{y}\cos\beta(\partial u_r/\partial r)] \tag{21b}$$

where

$$\hat{\varepsilon}_m = \partial \hat{u}_x^{\text{def}}/\partial\hat{x} \tag{22}$$

and for the transverse cubic displacement field

$$\hat{\phi}(\hat{x}) = (\hat{\phi}_1/l^2)(l^2 - 4l\hat{x} + 3\hat{x}^2) + (\hat{\phi}_2/l^2)(3\hat{x}^2 - 2l\hat{x}) \tag{23}$$

Equation (21b) is the standard equation for circumferential strains as given by Novozhilov,[12] whereas Eq. (21a) can be shown to be equivalent to that of Novozhilov within second-order terms in $\hat{\varepsilon}_m$ and $\partial\hat{\phi}/\partial\hat{x}$; both terms are small for moderate rotations if the strains are small.

The stresses are then computed by the usual engineering stress-strain laws. The equations for internal nodal forces corresponding to Eq. (9) are

$$\begin{Bmatrix} m^p_1 \\ m^p_2 \\ \hat{f}^p_{2x} \end{Bmatrix} = -\frac{1}{l^2} \int_{V_l} \begin{bmatrix} (6\hat{x} - 2l)\hat{y} \\ (6\hat{x} - 4l)\hat{y} \\ -l \end{bmatrix} \hat{\sigma}_x dV \tag{24}$$

Gaussian quadrature formulas were used to evaluate the above mentioned integrals with two points along the length and five points through the thickness. The other nodal forces are found by invoking the self-equilibration of the planar nodal forces

$$\hat{f}^p_{1y} = -\hat{f}^p_{2y} = (m^p_1 + m^p_2)/l \qquad \hat{f}^p_{1x} = -\hat{f}^p_{2x} \tag{25}$$

These nodal forces are then transformed into the global coordinates. The internal nodal forces due to the circumferential stresses are computed by the standard linear nodal force-stress relations.

For both elements, lumped masses are used. In the axisymmetric triangular element, the total mass is apportioned equally among the three nodes. In the conical shell element, the translatory and rotatory lumped mass at each node is equivalent to the mass and mass moment, respectively, of the segment between the node and the midpoint of the element. Inertia due to rotation of the cross section is neglected.

IV. Results

Results are presented here for three problems. The first two are circular plates clamped at the outer periphery and loaded impulsively at the center. Experimental and finite-difference results for these problems have been reported by Duffey and Key.[13] The experiment is depicted in Fig. 3. The clamping was effected by 12 $\frac{1}{2}$ in. bolts pretorqued to 85 ft-lb. It was not clear

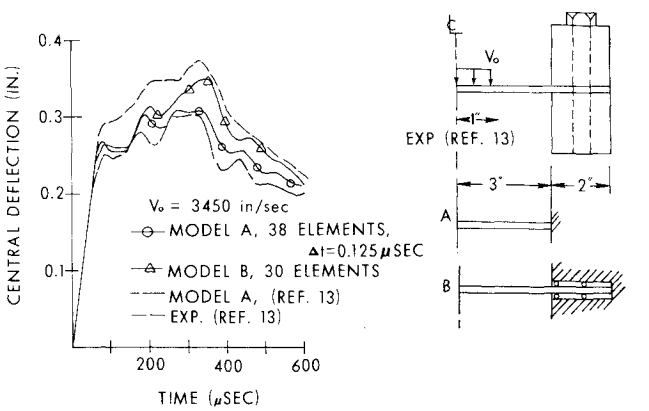

Fig. 3 Comparison of central deflection for $\frac{1}{16}$ in. steel plate with experimental and previously computed results.

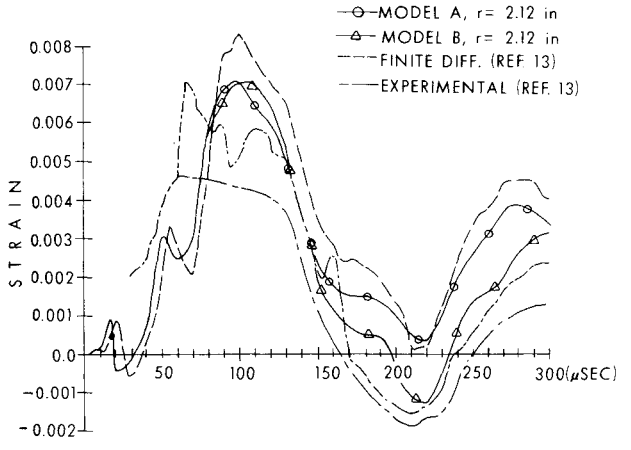

Fig. 4 Comparison of meridional strains for $\frac{1}{16}$ in. steel plate with experimental and previously computed results.

whether this setup effectively clamped the plate at the inner edge of the clamp. Plate slippage was also recognized as the principal source of experimental error by the authors of Ref. 13. Hence the two finite element models shown in Fig. 3, designated models A and B, were used. In the first model, the plate was clamped at the 3 in. radius, while in the second model the plate was supported by rollers over the outer 2 in. and clamped at the 5 in. radius. The second model is also only a rough approximation to the actual support. From the viewpoint of radial membrane wave propagation, the actual support consists of a fixed support over a part of the circumference and a free boundary over the remainder. Furthermore, before the onset of significant thinning due to plastic stretching of the plate, the clamping rings probably exert significant tangential forces on the plate; these are neglected in model B.

The material was assumed to be elastic-plastic. Between the yield stress σ_o and the ultimate stress σ_u, isotropic strain hardening with a constant plastic modulus E_p was assumed. Beyond the ultimate stress the material was assumed to be perfectly plastic. No strain rate effects were included. The material properties are listed in Table 1; the values for 6016-T6 aluminum and 1022 steel were taken directly from Ref. 13.

The central deflections as computed here, in Ref. 13, and observed experimentally, are shown in Fig. 3. Both models A and B have 30 elements over the inner 3 in. of the mesh. The results of model A compare very well with the results obtained in Ref. 13 by the finite-difference program. The slight differences may be ascribed to the difference in number of mesh points and number of points used in integrating through the thickness of the plate (4 were used in Ref. 13, 5 herein). It can also be seen that the results of model B compare more closely with the experimental results at later times, which supports the conjecture that sliding takes place between the clamp and the plate.

Figure 4 compares the meridional strain at $r = 2.0$ in. Two experimental curves are given in Ref. 13 and both are shown here. Again the finite-difference and finite element results for model A compare very well with each other and the experimental results. The results for model B obtained here more closely approximate the experimental results at later times. In addition, the peak strain obtained here matches one of the experimental peaks, though the significance of this is not clear since the two experimental peaks differ by about 30%. These differences may be due to asymmetries in the experiments introduced by the bolts. The strain gage was located 2 in. from the closest bolt and about 3 in. from the next closest bolt. Hence the reflection of stress waves from the bolts probably introduced a complicated three-dimensional wave pattern at the strain gage, which cannot be reproduced by an axisymmetric analysis. The effect of these asymmetries on the central deflection would be far smaller because of the equidistance of the bolts from the center.

Figure 5 compares the central deflection for a $\frac{1}{8}$-in.-thick aluminum plate loaded impulsively with experimental results reported in Ref. 13. Results are reported for three meshes to show the rate of convergence. In addition, the finite element results reported by Stricklin et al.[1] are shown. All of the computed results were obtained with a B-type mesh. Results obtained by the finer meshes and those given in Ref. 1 compare very well with the experiment for the first 400μsec. Subsequently, the results of Ref. 1 diverge somewhat from the experimental results. This should not be interpreted in any sense as indicating the superiority of one method over another. In order to accurately predict the response in the unloading phase, precise models of the material behavior under cyclic loadings are needed. Since both programs use a simple isotropic hardening stress-strain law, the better agreement of our analysis may be fortuitous.

The third problem, as shown in Fig. 6, consists of two concentric cylindrical shells separated by a layer of sodium. The geometry is symmetric about the lower horizontal axis and both the shells and sodium are unconstrained at the ends. Each shell was modelled by six flexural elements, while the sodium was represented by a single layer of twelve triangular continuum elements. The sodium nodes were rigidly connected to the shell nodes. As indicated in Table 1, the sodium was assumed to resist only compressive dilatations. In tension, the bulk modulus was taken to be zero. The problem was also repeated with the sodium elements free to slide tangentially relative to the shells; this hardly affected the results in the first cycle and by less than 10% in subsequent oscillations.

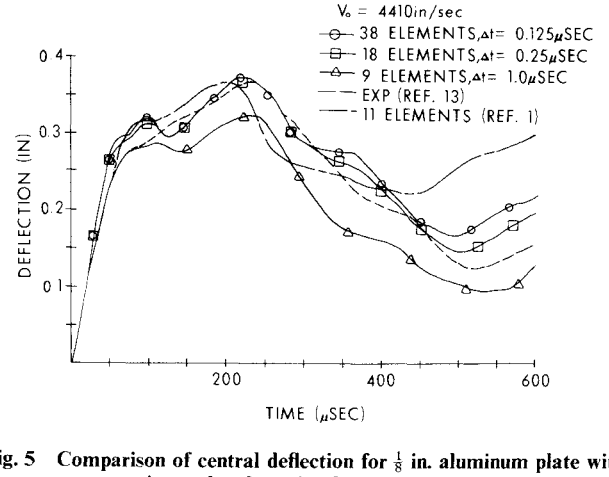

Fig. 5 Comparison of central deflection for $\frac{1}{8}$ in. aluminum plate with experimental and previously computed results.

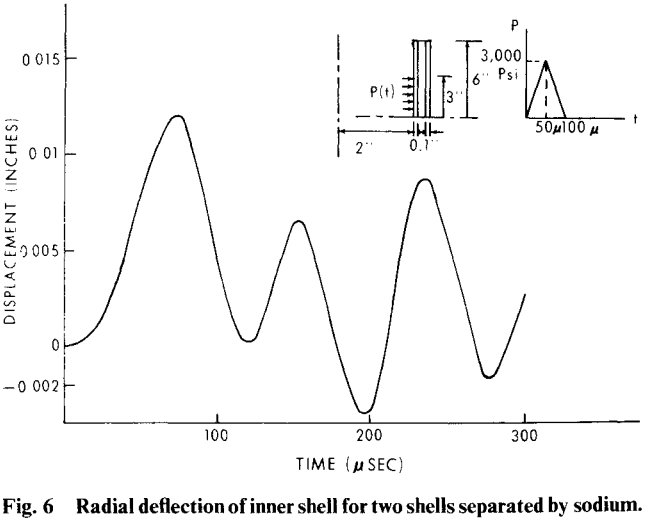

Fig. 6 Radial deflection of inner shell for two shells separated by sodium.

Table 1 Material properties

	E, Young's modulus, psi	σ_o, yield strength, psi	E_p, plastic modulus, psi	σ_u, ultimate stress, psi	Density, lb-sec^2/in.^{4}	Poisson's ratio
6061-T6 Aluminum (Fig. 5)	1.04×10^7	42,400	54,400	44,900	2.51×10^{-4}	0.3
1022 Steel (Figs. 3 and 4)	2.842×10^7	81,000	53,500	90,000	7.29×10^{-4}	0.3
Stainless steel (Fig. 6)	2.2×10^7	75,000	6.0×10^5	∞	7.3×10^{-4}	0.3
Sodium (Fig. 6)	bulk modulus = 5.88×10^5 in compression bulk modulus = 0.0 in tension			*	7.72×10^{-5}	*

V. Conclusions

A formulation and computer program have been described for the nonlinear analysis of axisymmetric shells and continua under dynamic loadings. Both material and geometric nonlinearities are included, though the latter is restricted to small strains and small variations of rotations within an element. A particular feature of this finite element procedure is the use of convected coordinates which rotate but do not deform with the element. It has been shown that the resulting finite element equations are simplified markedly, thereby providing significant computational advantages in transient calculations. The governing equations were solved in time by explicit integration and a lumped, diagonal mass matrix was used. This combination is ideally suited for large-scale analysis, since the computational effort increases only linearly with the number of nodes. By comparison, implicit integration schemes are bandwidth dependent; the number of computations is proportional to the product of the number of nodes and the square of the bandwidth.

The method was compared to experimental results and previous finite-difference and finite element computations. On the whole, all of the methods compared quite well with each other and the experimental results. However, some substantial differences were noted in the finite element results, particularly at later times. Because of the many idealizations involved in the transition from experiment to numerical model, the experimental results could not be used to judge the comparative accuracy of the methods. Exact solutions are not available. Hence, there is clearly a need for "benchmark" problems in the area of nonlinear transient analysis for the purpose of assessing new techniques and programs.

References

[1] Stricklin, J. A., Haisler, W. E., and Von Riesemann, W. A., "Computation and Solution Procedure for Nonlinear Analysis by Combined Finite Element-Finite Difference Methods," *Computers and Structures*, Vol. 2, 1972, pp. 955–974.

[2] Krieg, R. D. and Key, S. W., "Transient Shell Response by Numerical Time Integration," *Advances in Computational Methods in Structural Mechanics and Design*, edited by J. T. Oden et al., Univ. of Alabama in Huntsville Press, Huntsville, Ala., 1972, pp. 237–255.

[3] Oden, J. T., *Finite Elements of Nonlinear Continua*, McGraw-Hill, New York, 1972.

[4] Stricklin, J. A., Martinez, J. E., Tillerson, J. R., Hong, J. H., and Haisler, W. E., "Nonlinear Dynamic Analysis of Shells of Revolution by Matrix Displacement Methods," *AIAA Journal*, Vol. 9, No. 4, April 1971, pp. 629–636.

[5] McNamara, J. F. and Marcal, P. V., "Incremental Stiffness Method for Finite Element Analysis of the Nonlinear Dynamic Problem," *Numerical and Computer Methods in Structural Mechanics*, edited by S. J. Fenves et al., Academic Press, New York, 1973, pp. 353–376.

[6] Wu, R. and Witmer, E. A., "Finite-Element Analysis of Large Elastic-Plastic Transient Deformations of Simple Structures," *AIAA Journal*, Vol. 9, No. 9, Sept. 1971, pp. 1719–1724.

[7] Hartzman, M. and Hutchinson, J. R., "Non-Linear Dynamics of Solids by the Finite Element Methods," *Computers and Structures*, Vol. 2, 1972, pp. 47–77.

[8] Belytschko, T. and Hsieh, B. J., "Nonlinear Transient Finite Element Analysis with Convected Coordinates," *International Journal for Numerical Methods in English*, Vol. 7, 1973, pp. 255–271.

[9] Argyris, J. H., Kelsey, S., and Kamel, H., "Matrix Methods of Structural Analysis: A Precis of Recent Developments," *Matrix Methods of Structural Analysis*, edited by B. Fraejis deVeubeke, AGARDograph 72, Pergamon Press, New York, 1964, pp. 1–164.

[10] Wempner, G. A., "Finite Elements, Finite Rotations, and Small Strains of Flexible Shells," *International Journal of Solids and Structures*, Vol. 5, 1969, pp. 117–153.

[11] Murray, D. W. and Wilson, E. L., "Finite Element Large Deflection Analysis of Plates," *Journal of the Engineering Mechanics Division, ASCE*, Vol. 95, 1969, pp. 143–165.

[12] Novozhilov, V. V., *Foundations of the Nonlinear Theory of Elasticity*, Graylock Press, Rochester, N.Y., 1956.

[13] Duffey, T. A. and Key, S. W., "Experimental-Theoretical Correlations of Impulsively Loaded Clamped Circular Plates," *Experimental Mechanics*, Vol. 9, June 1969, pp. 241–249.